Unraveling the excited-state vibrational cooling dynamics of chlorophyll-a using femtosecond broadband fluorescence spectroscopy ⊘

Heyuan Liu ; Meixia Ruan ; Pengcheng Mao; Zhuan Wang ; Hailong Chen ✉ ; Yuxiang Weng

Check for updates

View Online   Export Citation

Unraveling the excited-state vibrational cooling dynamics of chlorophyll-a using femtosecond broadband fluorescence spectroscopy

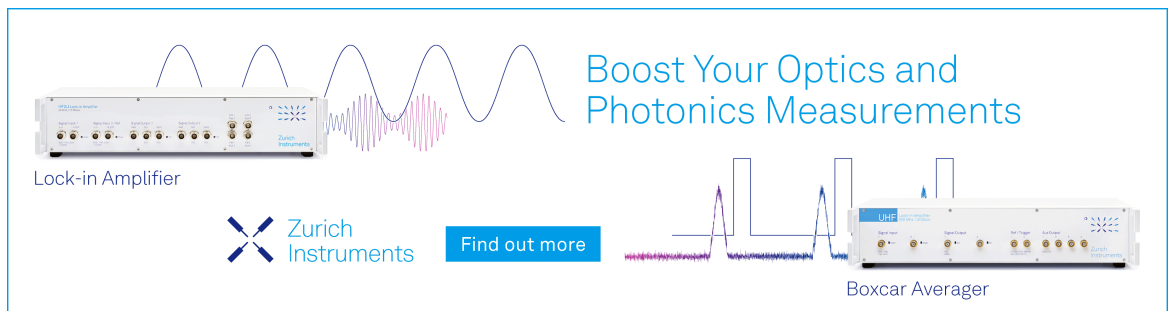View Online   Export Citation   CrossMark

Heyuan Liu,[1,2] (iD) Meixia Ruan,[1,2] (iD) Pengcheng Mao,[3] Zhuan Wang,[1] (iD) Hailong Chen,[1,2,4,a)] (iD) and Yuxiang Weng[1,2,4] (iD)

AFFILIATIONS

[1] The Laboratory of Soft Matter Physics, Beijing National Laboratory for Condensed Matter Physics, Institute of Physics, Chinese Academy of Sciences, Beijing 100190, China
[2] School of Physical Science, University of the Chinese Academy of Sciences, Beijing 100049, China
[3] Analysis and Testing Center, Beijing Institute of Technology, Beijing 100081, China
[4] Songshan Lake Materials Laboratory, Dongguan, Guangdong 523808, China

Note: This paper is part of the JCP Special Topic on Light-matter Interaction at the Nano and Molecular Scale.
[a)] Author to whom correspondence should be addressed: hlchen@iphy.ac.cn

ABSTRACT

Understanding the dynamics of excited-state vibrational energy relaxation in photosynthetic pigments is crucial for elucidating the mechanisms underlying energy transfer processes in light-harvesting complexes. Utilizing advanced femtosecond broadband transient fluorescence (TF) spectroscopy, we explored the excited-state vibrational dynamics of Chlorophyll-a (Chl-a) both in solution and within the light-harvesting complex II (LHCII). We discovered a vibrational cooling (VC) process occurring over ~6 ps in Chl-a in ethanol solution following Soret band excitation, marked by a notable ultrafast TF blueshift and spectral narrowing. This VC process, crucial for regulating the vibronic lifetimes, was further elucidated through the direct observation of the population dynamics of higher vibrational states within the Q_y electronic state. Notably, Chl-a within LHCII demonstrated significantly faster VC dynamics, unfolding within a few hundred femtoseconds and aligning with the ultrafast energy transfer processes observed within the complex. Our findings shed light on the complex interaction between electronic and vibrational states in photosynthetic pigments, underscoring the pivotal role of vibrational dynamics in enabling efficient energy transfer within light-harvesting complexes.

I. INTRODUCTION

In green plants, the primary light-harvesting complex of photosystem II (LHCII) functions as the principal solar energy collector, channeling sunlight energy toward the reaction center of the photosystem.[1,2] Chlorophylls (Chls), the predominant pigments in LHCII, are pivotal for fast excitation energy transfer (EET) with near-unity quantum efficiency. Despite extensive investigations into the ultrafast energy-transfer dynamics among Chls in LHCII, the intricate mechanism underlying EET remains elusive.[3–7] Recent studies recognize electronic–vibrational (vibronic) mixing as a facilitator for rapid EET between Chls, adding complexity to the understanding.[8–11] Arsenault et al. revealed that energy flows in LHCII from higher-lying electronic–vibrational mixing states to lower-lying chlorophyll states, enhancing the energy transfer rate.[10] In addition, Zhu et al. identified a 340 cm^{-1} out-of-plane vibration strongly coupled to the Q_y electronic state of Chl-a, modulating inter-pigment interactions in LHCII and leading to a more efficient energy transfer process.[11] Consequently, the involvement of vibrations in photo-excited Chls becomes pivotal in EET within light-harvesting complexes through vibronic coupling or other underlying steps. Emphasizing these aspects provides a deeper insight into such an efficient process.

Photo-induced processes in LHCII, such as EET, internal conversion, or the direct excitation of a vibronic transition, are always accompanied by a substantial excess of vibrational energy

29 May 2024 03:21:22

stored in the electronic excited states of Chls. Typically, the excited-state vibrational energy relaxation (VER) of a molecule involves two primary steps: intramolecular vibrational redistribution (IVR) and vibrational cooling (VC), which have been extensively studied in dye molecules.[12–16] The VC process is crucial for returning a vibrationally excited molecule to thermal equilibrium with its surroundings, comprising multiple sequential and parallel VER steps.[17,18] The cooling rate relies heavily on intermolecular interactions, encompassing interactions with neighboring solvent molecules and the intermolecular EET process. It plays a pivotal role in constraining the vibrational lifetimes in the electronic excited states. Despite research on VC dynamics in other systems, there is a notable lack of studies reporting on VC dynamics in photosynthetic pigments or complexes following photoexcitation.

Kosumi et al. conducted an in-depth exploration of the ultrafast VER dynamics of Mg- and Zn-bacteriochlorophyll-a using pump–probe spectroscopy.[19] They attributed sub-picosecond and 1.5 ps components to IVR and intermolecular VC between bacteriochlorophyll-a and surrounding solvents. However, transient absorption (TA) spectra in these studies are often convoluted with various components, hindering the direct spectral differentiation of VC from other intricate ultrafast photoinduced processes. In contrast, transient fluorescence (TF) measurements offer a direct means to probe excited states by monitoring changes in emission spectra, providing significant advantages in intuitively revealing VER processes.[16,20–25] Due to the relatively low fluorescence quantum yield of pigment molecules such as Chls compared to dye molecules,[26] the fluorescence characteristics of photosynthetic pigments have received limited attention. Dietzek et al. utilized a streak camera with high photoelectric conversion efficiency to successfully resolve the VER of the specific excited state of protochlorophyllide-a in both spectral and kinetic regimes.[22] They associated the 3.5 ps rise component with the VC of the hot S_1 state. Nevertheless, the detailed VER dynamics are constrained by the limited temporal resolution of streak cameras, typically on the picosecond time scale. Therefore, leveraging femtosecond TF spectroscopy to uncover the VC dynamics of photosynthetic pigments, particularly in light-harvesting complexes, promises a deeper understanding of VER mechanisms and valuable insights into the role of electronic–vibrational mixing states in ultrafast EET processes.

Utilizing upgraded fluorescence non-collinear optical parametric amplification spectroscopy (FNOPAS), we conducted a comprehensive examination of the excited-state VC dynamics of Chl-a in solution and LHCII at room temperature. Benefiting from the ultra-broad spectral bandwidth and sub 100 fs time resolution of FNOPAS,[27–35] we directly traced the ultrafast temporal evolution of the TF spectra of Chl-a in solution and LHCII following photoexcitation. We demonstrate ~6 ps excited-state VC dynamics in Chl-a solution following Soret band excitation, leading to a narrower TF spectrum and a blueshift in the band maximum. Furthermore, the VC-induced population dynamics of higher-quanta vibrational states in the Q_y electronic state are directly observed with femtosecond mid-infrared (MIR) TA spectroscopy. In contrast, the Chl-a in LHCII presents much faster VC dynamics within hundreds of femtoseconds, aligning with the timescale of the ultrafast EET process in LHCII. It indicates the higher-quanta electronic–vibrational mixing states of chlorophyll-a could effectively participate in the EET process of LHCII.

II. MATERIALS AND METHODS

A. Sample preparation

Chl-a powder, extracted from *Anacystis nidulans* algae, was purchased from Sigma-Aldrich. For ultrafast measurements, Chl-a was dissolved in an anhydrous ethanol solution with concentrations ranging from 1×10^{-4} to 1×10^{-5} mol/l and in chloroform at a concentration of 5×10^{-5} mol/l. Trimeric LHCII from spinach was extracted, isolated, and purified following previously established protocols.[36,37] The purified sample underwent freeze-drying and was stored at $-20\,^\circ$C until immediately before use. For TF measurement, LHCII proteins were dissolved in a 10 mM Tris-HCl buffer (pH 7.5) containing 0.03% β-dodecylmaltoside (β-DM) to an optical density of 0.38 at the Q_y band maximum (675 nm) in a 1 mm thick fused silica cuvette.

B. Steady-state characterizations

Steady-state absorption spectra were acquired using a custom UV–vis–near-infrared (NIR) spectrophotometer, with the sample enclosed in a 1 mm thick fused silica cuvette. For steady-state fluorescence spectra, a fluorescence spectrophotometer (FLS1000, Edinburgh Instruments) was employed under 400 nm laser excitation, utilizing samples within a 1 cm thick fused silica cuvette. The samples were diluted to achieve the same optical density as the 1 mm cuvette. All measurements were performed at room temperature.

C. Femtosecond time-resolved spectroscopies

1. Femtosecond broadband TF spectroscopy

The fundamental optical design of FNOPAS has been extensively elucidated in our previous studies.[28,29,32,33] Briefly, femtosecond pulses (800 nm, 100 fs, 2 kHz) generated from a Ti:sapphire amplifier (Solstice, Spectra-Physics) were divided into two beams using a 50/50 beam splitter. One beam was frequency-doubled through a 2 mm thick β-barium borate (BBO) crystal to generate a 400 nm laser, serving as the FNOPAS pump pulses. The other beam drove an optical parametric amplifier (TOPAS, Spectra-Physics) for tunable excitation pulses, which were then modulated by a mechanical optical chopper at 1 kHz. The energy of the excitation pulse at the sample was maintained below 0.15 μJ/pulse. The generated fluorescence from the sample was collected and focused onto a 1 mm thick BBO crystal (cut at θ = 31.5°, α = 0°), and subsequently amplified by the 400 nm pump pulses. The amplified fluorescence, along with the intrinsic parametric super-fluorescence (PSF) noise, was collected using an achromatic lens and coupled into an optical fiber connected to the spectrometer (Avaspec-ULS2048CL, Avantes). The amplified TF from the sample was acquired by subtracting the PSF background using the optical chopper. Correction for the distortion in the amplified fluorescence, stemming from the nonuniform gain curve inherent to the nonlinear optical crystal, was achieved by employing the corresponding PSF spectrum (see Fig. S2 in the supplementary material). Traditional FNOPAS measurements often encounter interference from the concurrent PSF background, significantly impacting the detection limit for capturing TF spectra of extremely weak fluorescence. In this study, to enhance fluorescence collection efficiency and reduce PSF noise fluctuations, we implemented a conical fluorescence collection and ring-like amplification configuration, replacing the conventional

lateral fluorescence collection and dot-like parametric amplification. This modification has been shown to yield an approximate order of magnitude reduction in PSF noise compared to previous FNOPAS setups.[38]

The time delay between the excitation and pump beams was precisely controlled using a monitored delay stage. To characterize the temporal resolution of FNOPAS, we utilized broadband supercontinuum white light as the seeding beam for the amplification process. Subsequently, the instrumental response function (IRF) was established based on the temporal characteristics of the broadband supercontinuum white light. This analysis revealed a full width at half maximum (FWHM) of less than 120 fs across the entire spectral range spanning from 500 to 720 nm (see Fig. S3 in the supplementary material). Throughout the measurements, the solution was continuously stirred within a 1 mm thick fused silica cuvette.

For TF anisotropy measurements, a quarter-wave plate was positioned in front of the sample to adjust the relative polarization between the excitation beam and the amplified fluorescence. By analyzing the collected TF intensities under parallel ($I_\parallel$) and perpendicular ($I_\perp$) polarization schemes, the anisotropy decay curve could be calculated using the formula $r(t) = [I_\parallel(t) - I_\perp(t)]/[I_\parallel(t) + 2I_\perp(t)]$.

2. Femtosecond MIR TA spectroscopy

The detailed description of femtosecond MIR spectroscopic measurement has been described elsewhere.[39–42] In summary, a femtosecond amplifier laser system (Spitfire Ace, Spectra-Physics) was utilized, generating 35 fs laser pulses centered at 800 nm with a repetition rate of 1 kHz. These laser pulses were split into two beams: the first beam pumped an optical parametric amplifier (TOPAS, Spectra-Physics), producing wavelength-tunable femtosecond pulses for sample excitation. The second beam was directed to generate MIR supercontinuum pulses for probing, achieved by simultaneously focusing the 800 nm fundamental light and its second harmonic light at 400 nm into the air. Both pump and probe pulses were focused onto the sample, which was contained in a CaF$_2$ flow cell with a 100 μm optical path. The detection of the MIR probe light was performed using a liquid-nitrogen-cooled, 64-channel mercury–cadmium–telluride-coupled spectrometer (FPAS-0144, Infrared Systems Development Corporation). The time delay between the pump and probe beams was precisely controlled using a monitored delay stage.

For both femtosecond TF and TA spectroscopies, a magic angle (54.7°) detection configuration was adopted to mitigate the effects of rotational relaxation, except for the polarization-dependent TF measurement. All experiments were conducted under ambient room temperature conditions.

III. RESULT AND DISCUSSION

A. Steady-state spectral characterization

Figure 1(a) shows the steady-state absorption and fluorescence spectra of Chl-a in an ethanol solution at a concentration of 5×10^{-5} mol/l at room temperature. According to Gouterman's classical four-orbital model theory,[43] molecules with a porphyrin skeleton such as Chl-a exhibit two prominent absorption bands in the violet and red regions, named the Soret and Q$_y$ bands, respectively.[44] The Soret band, the highest-lying electronic band, peaks at 430 nm, while the peak at 664 nm is attributed to the Q$_y$ 0 → 0 transition. The corresponding steady-state fluorescence, excited by a 400 nm laser, peaks at 675 nm, which is assignable to emission from Q$_y$.[19] It resembles a mirror symmetry to the absorption spectrum, although with slight differences and a modest Stokes shift of ~397 cm^{-1}. The breakdown of the mirror symmetry can be explained by the Frank–Condon and Hertzberg–Teller interactions in Chl-a.[19] The far-red "shoulder" structure centered at 728 nm is ascribed to the 0 → 1 vibronic transition from Q$_y$ to ground state.[45] The steady-state absorption spectra of Chl-a in ethanol solution at different concentrations are provided in the supplementary material (Fig. S1).

The trimeric LHCII pigment–protein complexes extracted from spinach typically contain eight Chl-a, six Chl-b, and four carotenoid pigment molecules in each monomer.[46,47] The steady-state absorption of LHCII solution, depicted in Fig. 1(b), features a strong violet absorption band contributed by the Soret band of Chls, with two prominent peaks at 437 and 472 nm attributed to Chl-a and Chl-b, respectively. The Q$_y$ bands of Chl-a and Chl-b give rise to peaks at 651 and 674 nm in the red absorption region, respectively. The steady-state fluorescence, peaking at 684 nm, is contributed by the terminal emissive Chl-a chromophores.

B. VC dynamics of Chl-a in solution

Femtosecond TF measurements were first conducted on a 5×10^{-5} mol/l Chl-a ethanol solution, with excitation pulses tuned
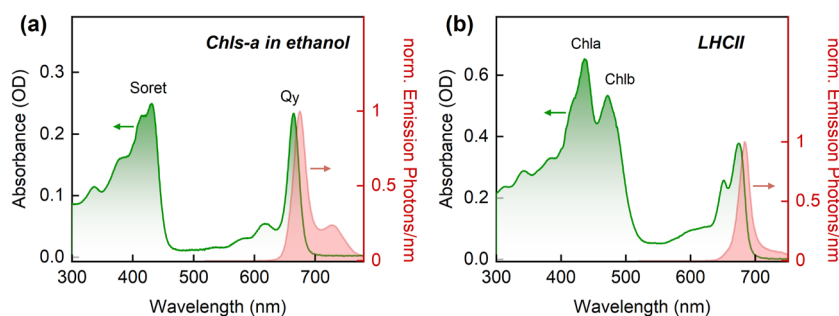

FIG. 1. Steady-state absorption and fluorescence (PL) characteristics of (a) Chl-a in ethanol solution and (b) LHCII sample.
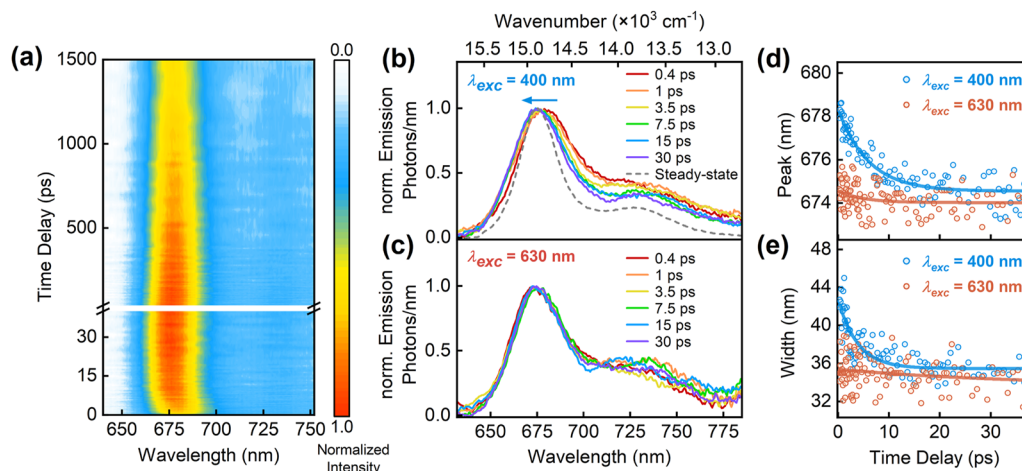
FIG. 2. (a) Waiting-time-dependent TF spectra of 5×10^{-5} mol/l Chl-a ethanol solution under 400 nm excitation. (b) TF spectra of Chl-a at various time delays and its steady-state fluorescence spectrum with the excitation wavelength (λ_{exc}) fixed at 400 nm. (c) TF spectra of Chl-a at various time delays under 630 nm excitation. (d) A comparison of the waiting-time-dependent TF peak under the Soret band (400 nm) and Q_y band (630 nm) excitations. (e) A comparison of the waiting-time-dependent TF spectral width under the Soret band (400 nm) and Q_y band (630 nm) excitations. In (d) and (e), the dots denote the data points, while the curves denote the single-exponential fitting.

resonantly to the Soret and Q_y bands of Chl-a, respectively. As depicted in Figs. 2(a) and 2(b), following Soret band excitation with 400 nm pulses, the waiting-time-dependent TF spectra of Chl-a are primarily dominated by the emission from the Q_y state, which can last for several nanoseconds. Remarkably, within 30 ps of photoexcitation, the TF peak gradually blueshifts, and the TF spectrum simultaneously undergoes a rapid spectral narrowing process and becomes more structured. In contrast, upon exciting the Q_y band of Chl-a with 630 nm pulses, the TF spectrum exhibits no discernible spectral change in both the emission maxima and the peak width, as shown in Fig. 2(c).

To quantitatively characterize the transient spectral shape changes, the lognormal function was adopted to fit the spectral line shape[48,49] (see Fig. S4 in the supplementary material). Figures 2(d)

and 2(e) present a comparison of the temporal evolution of the TF peak and TF spectral width under the Soret band and Q_y band excitations. Under Soret band excitation, the dynamics of peak shifting from 678 to 674.5 nm are well-described by a single-exponential function, characterized by a time constant of 5.9 ± 0.7 ps. Meanwhile, the TF spectra exhibit rapid narrowing dynamics from about 42–36 nm with a time constant of 3.8 ± 0.65 ps. In contrast, under Q_y band excitation, both the TF peak and TF spectral width show only minor changes. The TF peak remains centered around 674.5 nm, which is very close to that at tens of picoseconds after Soret band excitation.

We further compared the dynamic peak shift for Chl-a solutions with different molar concentrations under Soret band excitation. As presented in Figs. 3(a) and S5 in the supplementary material,
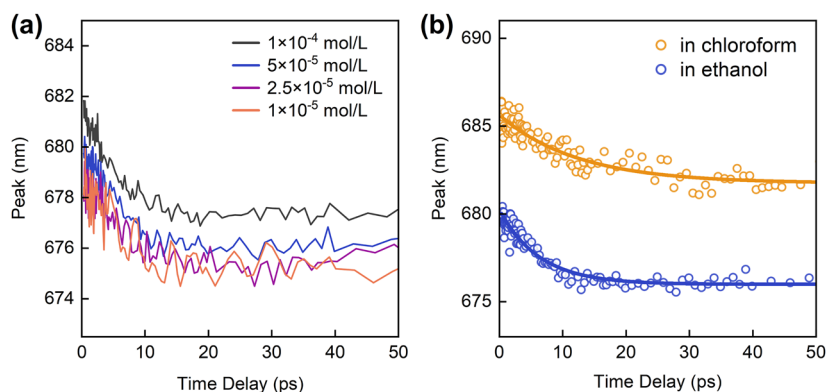

FIG. 3. (a) Waiting-time-dependent TF peak of Chl-a ethanol solution under 400 nm excitation at different concentrations. (b) A comparison of the waiting-time-dependent TF peak for 5×10^{-5} mol/l Chl-a ethanol solution and 5×10^{-5} mol/l chloroform solution under 400 nm excitation. The dots denote the data points, while the curves denote the single-exponential fitting.

there is no obvious concentration dependence of the blueshift and band narrowing dynamics across an order of magnitude from 10^{-4} to 10^{-5} mol/l. Only at a very high concentration (10^{-4} mol/l) does the TF peak shift about 2 nm to the red region, primarily due to the fluorescence self-absorption effect. We also compared the waiting-time-dependent TF peak for Chl-a dissolved in ethanol and in chloroform under the Soret band excitation. As presented in Fig. 3(b), the blueshift dynamics of the TF peak become noticeably slower in chloroform solution than in ethanol solution. A peak shifting time of 12.4 ± 1.6 ps can be obtained for the Chl-a chloroform solution. It indicates the observed dynamic peak shift phenomenon may strongly depend on the interactions between Chl-a and neighboring solvent molecules.

Previously, the ultrafast redshift of the TF spectrum was often observed for various dye molecules in solution and was generally interpreted as the consequence of the fast singlet excited state's energy reduction due to reorganization of the polar solvent molecules around the increased dipole moment following photoexcitation.[50,51] Since the observed emission spectral blueshift of Chl-a almost disappears under Q_y band excitation, these solvation effects can be excluded here. Moreover, the concentration-dependent measurements also exclude the possibility of aggregation-induced spectral shifts, such as the formation of excimer at higher concentrations.[33] Therefore, the observed emission maxima blueshift and spectral narrowing phenomenon most

likely arise from the VC process, previously observed in other molecular systems.[16,24,25]

In particular, subsequent to Soret band excitation of Chl-a, the internal conversion toward Q_y typically takes place within a few hundred femtoseconds, leading to rapid emission from the Q_y state. As shown in Fig. 4(a), an emission increasing process of around 300 fs can be obtained by fitting the rising edge of TF dynamics at all probe wavelengths. This ultrafast process corresponds to the internal conversion dynamics [see Fig. 4(b)], consistent with previous theoretical and experimental studies.[52–54] Along with the internal conversion, a large amount of vibrationally excess energy (VEE) is produced inside Chl-a. Following the IVR process, which is mainly via anharmonic coupling, the VEE is redistributed among other vibrational modes. Consequently, the excited-state population forms a canonical ensemble, thus defining a molecular temperature that can be significantly higher than that of the surrounding environment.[23] Then, the VC process takes place, where the "hot" Chl-a cools down by intermolecular interactions, such as energy transfer between Chl-a and neighboring solvent molecules.

Figure 4(b) provides an illustrative understanding of the fluorescence emission change of Chl-a due to the VC process based on the well-known Jablonski energy diagram, which describes the anharmonicity of specific vibrational modes on different potential energy surfaces. As for different electronic potential energy surfaces, there is closer spacing of adjacent vibrational levels in the
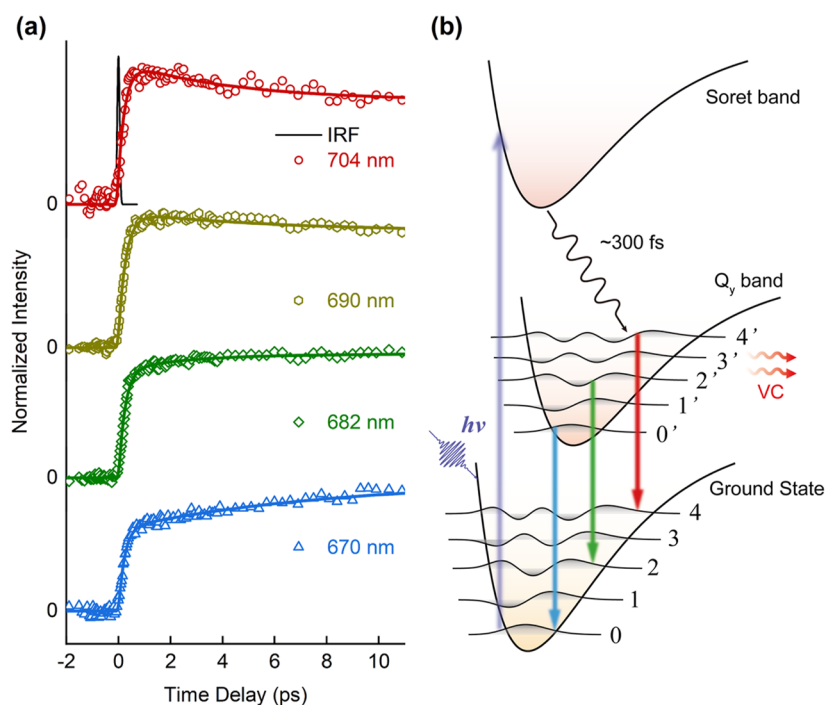

FIG. 4. (a) TF dynamics of Chl-a ethanol solution at different wavelengths under 400 nm excitation. The black curve co-existing in 704 nm dynamics represents the IRF. The dots denote the data points, while the curves denote the multi-exponential fitting, accounting for the IRF (~120 fs). (b) Schematic internal conversion, vibrational cooling, and fluorescence emission processes of Chl-a following Soret band excitation based on the Jablonski diagram. Since the spacing of adjacent vibrational levels in the Q_y band is smaller than that in the ground state (e.g., $v_{0'\to1'} < v_{0\to1}$), the average emission photon energy becomes larger during the VC process, resulting in the observed blueshift dynamics.

excited state than in the ground state for a specific mode quantum number,[25] e.g., $v_{0'\rightarrow1'} < v_{0\rightarrow1}$, which will be further confirmed by the following femtosecond MIR experiments. As a result, a higher-lying vibronic transition from Q_y to the ground state [e.g., the red arrow in Fig. 4(b)] corresponds to an emission with relatively smaller photon energy compared with that of a lower-lying vibronic transition [e.g., the green arrow in Fig. 4(b)]. During the VC process, the vibrational population of higher-quanta states gradually decreases, leading to a larger average emission of photon energy and fewer vibrationally excited modes. Therefore, the corresponding TF spectrum would be expected to blueshift and become narrower, which is in good accordance with our experimental observation [see Fig. 2(b)]. The VC dynamics can also be monitored from TF dynamics at different wavelengths, as plotted in Fig. 4(a). The dynamics at longer wavelengths exhibit a decaying profile, accompanied by a rising profile at shorter wavelengths, indicating more lower-quanta states are populated during the VC process.

In contrast, upon Q_y excitation, there is only a small amount of VEE compared with that for Soret band excitation.[19] In this situation, the molecule is not "hot" enough, and its vibrations initially populate lower-quanta states. A relatively unnoticeable amount of spectral narrowing and blueshift would be expected, as observed in Fig. 2(c). It is worth noting that the vibrationally cooled spectrum under 400 nm excitation still has a slightly red-shifted peak and broader width compared to that under 630 nm excitation over the time window of the experiment, as shown in Figs. 2(d) and 2(e). One possible reason is that, following 400 nm photoexcitation, a large amount of VEE produced in Chl-a is dissipated to surrounding solvent molecules, transiently heating the solution. The elevated temperature leads to a denser population distribution in the

higher-quanta vibrational states and cools down on a relatively longer time scale than the VC mediated process,[21] which may result in a subtle difference in the vibrationally cooled spectrum under different excitation wavelengths. However, our experimental result shows that the peak position difference after the VC process under two distinct excitation conditions lies within the fluctuation errors [see Fig. 2(d)], indicating the contribution from the elevated temperature of surrounding solvent molecules would be small. Moreover, a relatively faster VC dynamics of Chl-a in ethanol than that in chloroform, as shown in Fig. 3(b), can be attributed to the fact that the solute having H-bonding sites tends to favor vibrational energy relaxation of the excited molecule.[23]

Considering the rich vibration modes of Chl-a in the MIR spectral region,[55,56] we further conducted femtosecond MIR TA measurements to directly trace the VC induced vibrational population change of higher-quanta states in the Q_y band of Chl-a. Three excitation wavelengths of 400, 650, and 670 nm were employed to selectively excite the Soret band and the blue and red edges of the Q_y band, respectively, producing a certain amount of VEE. MIR TA spectra under 400 nm excitation are shown in Fig. 5(a). Two pairs of positive and negative peaks centered at 1634 and 1670, 1682 and 1699 cm^{-1} were observed in the spectral region from 1580 to 1740 cm^{-1} (see Fig. S6 in the supplementary material). The negative peak at 1670 cm^{-1} arises from ground state vibrational bleaching of C=O stretching modes of the ester groups,[56] i.e., the decreased $0 \rightarrow 1$ transition on the ground state of Chl-a upon photoexcitation. The positive signal around 1634 cm^{-1} is contributed by the increased vibrational absorption on the electronic excited state, including the $0' \rightarrow 1'$ transition shown in Fig. 4(b). The observed TA spectra indicate that, for a specific vibrational mode of Chl-a, the
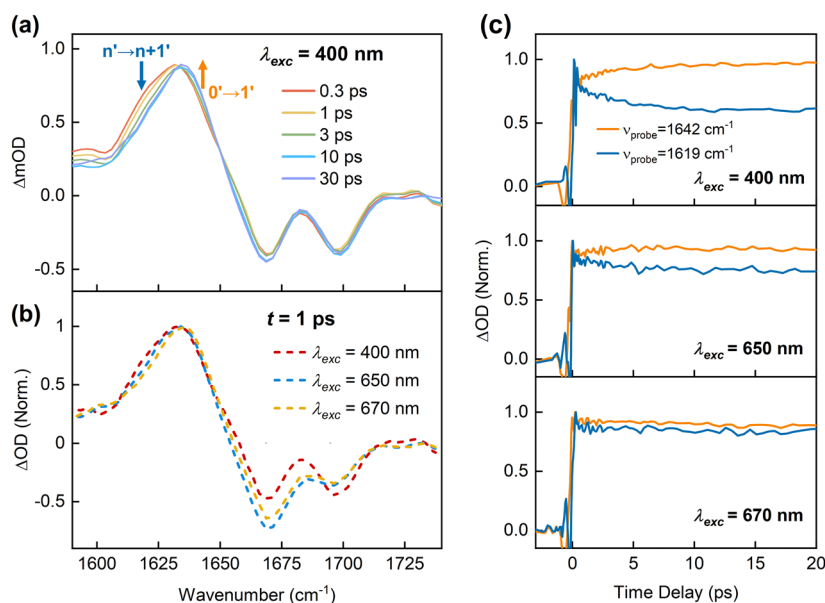

FIG. 5. (a) MIR TA spectra of Chl-a ethanol solution at various time delays under 400 nm excitation. (b) MIR TA spectra of Chl-a ethanol solution under excitation of different wavelengths, with the time delay t fixed at 1 ps. (c) TA dynamics of Chl-a ethanol solution probed at higher-quanta state (1619 cm^{-1}, blue lines) and lower-quanta state (1642 cm^{-1}, orange lines) under excitation of different wavelengths.

vibrational absorption signal has a lower frequency compared with the vibrational bleaching signal. It confirms closer spacing between adjacent vibrational levels on the Q_y band than on the ground state, as discussed above.

More importantly, we can observe that the spectral intensity rapidly decreases within tens of picoseconds at the lower frequency region of the positive signal around 1634 cm^{-1}, while that at the higher frequency region keeps increasing, as marked by the vertical arrows in Fig. 5(a). Subsequent to Soret band excitation, the internal conversion and IVR process in Chl-a finish within several femtoseconds. Then, the generated VEE is distributed among different vibrational modes in the Q_y state, including higher-quanta vibrational states. Due to the anharmonicity of vibrational levels within the electronic state, the photon energy for the transition from a higher-quanta state is generally smaller than that from a lower-quanta state, e.g., $1' \rightarrow 2'$ has a smaller energy gap than $0' \rightarrow 1'$.[57] Therefore, we can attribute the signal at the highest frequency region of the positive peak to the transition of $0' \rightarrow 1'$ and that at the lower frequency region to the superposition of transitions of $n' \rightarrow n + 1'$ ($n > 0$), as depicted in Fig. 5(a). Therefore, the temporal evolution of MIR TA spectra reflects the decreased vibrational population of higher-quanta vibronic states during the VC process, consistent with our TF results.

When the excitation light shifts to a longer wavelength, such as 650 or 670 nm, the population in higher-quanta states remarkably decreases following photoexcitation, as shown in Fig. 5(b). This contrast can be visually observed from the comparison of dynamics probed at the higher-quanta state (1619 cm^{-1}) and lower-quanta state (1642 cm^{-1}) under different excitation wavelengths. The results are plotted in Fig. 4(c), where the difference between these two dynamics becomes more unobvious under higher wavelength excitation. In particular, under 650 nm excitation into the blue edge of the Q_y band, only a relatively small amount of VEE was introduced, leading to a not too "hot" molecule. A similar dynamic profile to that for 400 nm excitation was observed, but with a relatively slower transition rate, reflected as a less prominent VC process. When further excitation of the red region of the Q_y band with 670 nm pulses occurs, the rapidly decaying component at 1619 cm^{-1} or rising component at 1642 cm^{-1} disappears and is replaced by a nearly synchronized decaying component that is commensurate with Q_y lifetime. In this situation, only the very low vibrational

quantum states near the bottom of the potential energy surface can be excited, and thus, the VC effect can be ignored.

C. VC dynamics of Chl-a in LHCII

The VEE of Chl-a excited in an ethanol solution predominantly dissipates through interactions with solvent molecules via the VC process. In natural environments, Chl-a are predominantly found within pigment–protein complexes, such as the LHCII antenna. To elucidate the VC dynamics of Chl-a in these natural light-harvesting antenna systems, femtosecond TF measurements were conducted on the LHCII sample. Excitation with 400 nm light preferentially excited the blue edge of the Soret band of Chl-a and the S_2 state of a subset of carotenoids. Given that this excitation wavelength significantly deviates from the absorption bands of Chl-b, the possibility of energy migration from Chl-b to Chl-a was considered negligible. The TF spectra of LHCII observed at various time delays following 400 nm excitation, as depicted in Fig. 6(a), are predominantly characterized by emission from the Q_y state of Chl-a. Notably, within a mere 1 ps, significant variations in both the central wavelength and the peak width of the TF spectrum were observed, which subsequently remained largely stable over tens of picoseconds. Figure 6(b) offers a comparative analysis of the waiting-time-dependent TF peak for Chl-a in ethanol solution vs within LHCII upon 400 nm excitation. Contrary to the observations in solution, Chl-a within LHCII exhibits markedly faster VC dynamics, confined to the timescale of hundreds of femtoseconds. This indicates that the VEE dissipation of Chl-a within LHCII follows distinct VC pathways, diverging from the conventional pigment–solvent interaction mechanism.

In the LHCII, Chl-a are intricately arranged in a circular pattern within the protein backbone, with an average center-to-center inter-pigment distance of ~11.26 Å.[46] This configuration establishes a broad energy transfer network. To elucidate the EET process among Chl-a within LHCII, TF anisotropy measurements were conducted on both Chl-a solution and LHCII, as depicted in Fig. 6(c). Initially, the TF anisotropy value for Chl-a solution is ~0.2, indicating a cross angle of about 35° between the transition dipole moments of the excited Soret state and the detected Q_y state.[58,59] Subsequently, the anisotropy decays to zero with a time constant of 290 ± 40 ps (see Fig. S7 in the supplementary material), a process
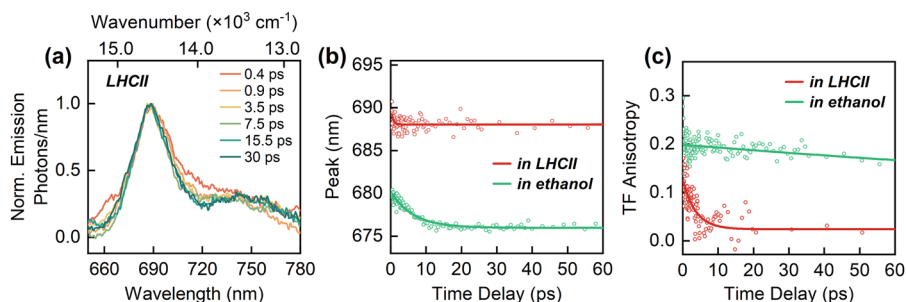

FIG. 6. (a) TF spectra of Chl-a in LHCII at various time delays under 400 nm excitation. (b) A comparison of the waiting-time-dependent TF peak for Chl-a in ethanol solution and LHCII under 400 nm excitation. (c) TF anisotropic dynamics of Chl-a in ethanol solution detected at 681 nm and Chl-a in LHCII detected at 687 nm. In (b) and (c), the dots denote the data points, while the curves denote the single-exponential fitting.

predominantly governed by the rotational motion of Chl-a, which typically occurs on the order of hundreds of picoseconds and is influenced by molecular size.[60] In stark contrast, the TF anisotropy in LHCII exhibits a much faster decay, incorporating a rapid component within hundreds of femtoseconds and a process lasting ~4 ps. This phenomenon was also observed previously with the femtosecond fluorescence up-conversion apparatus, where the fluorescence anisotropy of LHCII decays with components of 250 fs and ~5 ps, attributed to the intermolecular EET process.[61] The variance in decay timescales suggests the coexistence of both strong and weak coupling among Chl-a molecules within LHCII, which is critical for facilitating EET dynamics.

Thus, chlorophyll-a molecules photoexcited by the Soret band exciton can rapidly undergo cooling via intermolecular EET within LHCII, as evidenced in Fig. 6(b). Crucially, this indicates that the higher-lying vibrational states in the electronic excited state of Chl-a are actively involved in the ultrafast EET process, occurring within hundreds of femtoseconds. This finding implies that the slow relaxation of intramolecular vibrational modes in the electronic excited state of Chl-a may play a pivotal role in natural light harvesting, potentially accelerating energy transfer dynamics. Further detailed investigation is required to fully understand the underlying physical mechanisms of this process.

IV. CONCLUSIONS

In conclusion, our study offers a comprehensive understanding of the excited-state VC dynamics of Chl-a both in solution and within the LHCII through advanced femtosecond broadband TF spectroscopy. We observed an ~6 ps VC process in Chl-a in ethanol solution following Soret band excitation, characterized by a rapid blueshift and narrowing of the TF spectrum. The VC dynamics exhibit a strong dependence on excitation photon energy and the interaction between Chl-a and surrounding solvent molecules. In addition, femtosecond MIR TA spectroscopy revealed the population dynamics of C=O stretching modes on higher vibrational states within the Q_y electronic state, providing visual evidence of the efficient VC process. In contrast, Chl-a in LHCII exhibited much faster VC dynamics within a few hundred femtoseconds, consistent with the ultrafast energy transfer process within the complex. These findings underscore the potential significance of electronic–vibrational mixing states in photosynthetic pigments, which are crucial for ultrafast energy transfer processes within light-harvesting complexes. Our study contributes valuable insights into natural photosynthetic mechanisms and suggests promising directions for the development of more efficient artificial light-harvesting systems.

SUPPLEMENTARY MATERIAL

See the supplementary material for the steady-state absorption spectra of Chl-a in ethanol solution at different concentrations, spectral correction of the transient fluorescence spectrum, characterization of the temporal resolution of FNOPAS, lognormal fitting of the TF spectrum, TF dynamics of Chl-a solution with different concentrations; mid-infrared spectral characterization, and polarization dependent TF dynamics.

AUTHOR DECLARATIONS

Conflict of Interest

The authors have no conflicts to disclose.

Author Contributions

H.L. conducted the transient fluorescence measurements, while M.R. was responsible for the preparation of the LHCII sample.

Heyuan Liu: Data curation (lead); Formal analysis (lead); Investigation (lead); Methodology (equal); Visualization (lead); Writing – original draft (equal). **Meixia Ruan**: Formal analysis (equal); Resources (lead); Visualization (equal). **Pengcheng Mao**: Conceptualization (equal); Formal analysis (supporting); Investigation (equal). **Zhuan Wang**: Investigation (supporting); Methodology (supporting). **Hailong Chen**: Conceptualization (lead); Formal analysis (lead); Methodology (lead); Supervision (lead); Writing – original draft (lead). **Yuxiang Weng**: Conceptualization (equal); Methodology (equal); Supervision (equal).

DATA AVAILABILITY

The data that support the findings of this study are available from the corresponding author upon reasonable request.

REFERENCES

[1] R. E. Blankenship, *Molecular Mechanisms of Photosynthesis* (John Wiley & Sons, 2021).
[2] R. Croce and H. van Amerongen, Science **369**, eaay2058 (2020).
[3] I. Mukerji and K. Sauer, Biochim. Biophys. Acta, Bioenerg. **1142**, 311 (1993).
[4] G. Trinkunas *et al.*, J. Phys. Chem. B **101**, 7313 (1997).
[5] C. C. Gradinaru *et al.*, J. Phys. Chem. B **104**, 9330 (2000).
[6] X. Pan, Z. Liu, M. Li, and W. Chang, Curr. Opin. Struct. Biol. **23**, 515 (2013).
[7] A. Dingle, BSc (Hons) Projekverslag No. 79583, Rhodes University, 2014.

[8] N. H. C. Lewis et al., J. Phys. Chem. Lett. **7**, 4197 (2016).

[9] M. H. Lee and A. Troisi, J. Chem. Phys. **146**, 075101 (2017).

[10] E. A. Arsenault et al., Nat. Commun. **11**, 1460 (2020).

[11] R. Zhu et al., J. Chem. Phys. **156**, 125101 (2022).

[12] A. Weiner and E. Ippen, Chem. Phys. Lett. **114**, 456 (1985).

[13] T. Elsaesser and W. Kaiser, Annu. Rev. Phys. Chem. **42**, 83 (1991).

[14] S. Kovalenko, R. Schanz, H. Hennig, and N. Ernsting, J. Chem. Phys. **115**, 3256 (2001).

[15] J.-Y. Liu et al., J. Phys. Chem. A **107**, 10857 (2003).

[16] O. Braem, T. J. Penfold, A. Cannizzo, and M. Chergui, Phys. Chem. Chem. Phys. **14**, 3513 (2012).

[17] J. R. Hill and D. D. Dlott, J. Chem. Phys. **89**, 842 (1988).

[18] J. R. Hill et al., J. Chem. Phys. **88**, 949 (1988).

[19] D. Kosumi et al., J. Chem. Phys. **139**, 034311 (2013).

[20] A. Mokhtari, A. Chebira, and J. Chesnoy, J. Opt. Soc. Am. B **7**, 1551 (1990).

[21] K. Ohta, T. J. Kang, K. Tominaga, and K. Yoshihara, Chem. Phys. **242**, 103 (1999).

[22] B. Dietzek et al., ChemPhysChem **7**, 1727 (2006).

[23] A. Pigliucci, G. Duvanel, L. M. L. Daku, and E. Vauthey, J. Phys. Chem. A **111**, 6135 (2007).

[24] T. Yamaguchi, Y. Kimura, and N. Hirota, J. Chem. Phys. **113**, 2772 (2000).

[25] E. Vogt et al., J. Phys. Chem. Lett. **12**, 11346 (2021).

[26] L. S. Forster and R. Livingston, J. Chem. Phys. **20**, 1315 (1952).

[27] P. Fita, Y. Stepanenko, and C. Radzewicz, Appl. Phys. Lett. **86**, 021909 (2005).

[28] X. H. Chen, X. F. Han, Y. X. Weng, and J. Y. Zhang, Appl. Phys. Lett. **89**, 061127 (2006).

[29] X. F. Han, X. H. Chen, Y. X. Weng, and J. Y. Zhang, J. Opt. Soc. Am. B **24**, 1633 (2007).

[30] H. L. Chen, Y. X. Weng, and J. Y. Zhang, J. Opt. Soc. Am. B **26**, 1627 (2009).

[31] H. L. Chen, Y. X. Weng, and X. Y. Li, Chin. J. Chem. Phys. **24**, 253 (2011).

[32] H. Chen et al., Photosynth. Res. **111**, 81 (2012).

[33] P. Mao, Z. Wang, W. Dang, and Y. Weng, Rev. Sci. Instrum. **86**, 123113 (2015).

[34] W. Dang et al., Chin. Phys. B **25**, 054207 (2016).

[35] H. Liu et al., Chin. J. Chem. Phys. **36**, 655 (2023).

[36] H. Li et al., Sci. China Chem. **63**, 1121 (2020).

[37] S. Caffarri et al., EMBO J. **28**, 3052 (2009).

[38] E. Cui et al., Rev. Sci. Instrum. **95**, 033008 (2024).

[39] H. Zhao, Q. Zhang, and Y.-X. Weng, J. Phys. Chem. C **111**, 3762 (2007).

[40] M. Zhu, G. Zhu, and Y. Weng, Appl. Spectrosc. **67**, 506 (2013).

[41] G. Zhu, M. Zhu, and Y. Weng, Appl. Spectrosc. **68**, 1374 (2014).

[42] Z. Chi, H. Chen, Q. Zhao, and Y.-X. Weng, J. Chem. Phys. **151**, 114704 (2019).

[43] M. Gouterman, J. Mol. Spectrosc. **6**, 138 (1961).

[44] A. B. J. Parusel and S. Grimme, J. Phys. Chem. B **104**, 5395 (2000).

[45] M. Ratsep, J. Linnanto, and A. Freiberg, J. Chem. Phys. **130**, 194501 (2009).

[46] Z. F. Liu et al., Nature **428**, 287 (2004).

[47] M. Ruan et al., Nat. Plants **9**, 1547 (2023).

[48] J. Sung et al., Nat. Commun. **6**, 8646 (2015).

[49] X. X. Zhang et al., Rev. Sci. Instrum. **82**, 063108 (2011).

[50] S. Pommeret et al., J. Mol. Liq. **64**, 101 (1995).

[51] Q. Ding et al., Opt. Commun. **284**, 3110 (2011).

[52] Y. Shi, J. Y. Liu, and K. L. Han, Chem. Phys. Lett. **410**, 260 (2005).

[53] W. P. Bricker et al., Sci. Rep. **5**, 13625 (2015).

[54] P. M. Shenai et al., J. Phys. Chem. B **120**, 49 (2016).

[55] M. Ratsep, J. M. Linnanto, and A. Freiberg, J. Phys. Chem. B **123**, 7149 (2019).

[56] N. H. C. Lewis and G. R. Fleming, J. Phys. Chem. Lett. **7**, 831 (2016).

[57] V. O. Kompanets et al., JETP Lett. **92**, 135 (2010).

[58] M. Vangurp, G. Vanginkel, and Y. K. Levine, Biochim. Biophys. Acta, Bioenerg. **973**, 405 (1989).

[59] M. A. M. J. v. Zandvoort et al., Photochem. Photobiol. **62**, 299 (1995).

[60] S. Akimoto and M. Mimuro, Photochem. Photobiol. **83**, 163 (2007).

[61] M. Du, X. Xie, L. Mets, and G. R. Fleming, J. Phys. Chem. **98**, 4736 (1994).

29 May 2024 03:21:22